Journal of Data Acquisition and Processing
ISSN: 1004-9037
https://sjcjycl.cn/
DOI: 10.5281/zenodo.777811

A CLASSIFICATION OF RETINAL DISEASE USING KM-WS APPROACH WITH THE PDDLSTM CLASSIFIER

Sheeja Mary F
Research Scholar, Dept. of Computer Science and Engineering, Annamalai University
Annamalainagar – 608002, Email: zsheeja@yahoo.co.in

Dr. V. Asanambigai
Assistant Professor, Dept. of Computer Science and Engineering, Annamalai University
Annamalainagar – 608 002, Email: tradingbaskeran@gmail.com

Dr. A. Lenin Fred
Principal, Mar Ephraem College of Engineering and Technology, Marthandam
Email: leninfred.a@gmail.com

ABSTRACT

The computerized analysis of retinal fundus images can be used to conduct the early diagnosis of retinal abnormalities such as diabetic retinopathy (DR). The most major issues with DR detection include noise artefacts brought on by inappropriate lighting, the overlap of lesions and blood vessels because of their similar intensities, and missing data brought on by the processing of a huge quantity of data. This research presented a detection and classification of retinal disease using the KM-WS technique. The main processing phases of the developed DR detection model is Filtering, Segmentation of abnormalities, Feature extraction, Optimal feature selection, and Classification. At first, filter the noises using Block-Matching and 3D (BM3D) approach. The next phase performs the optic disc removal, which is carried out by Kirsch with Mask based Watershed Segmentation (KM-WS) is done for segmenting the blood vessels and its removal.Further, the feature extraction phase is started, which tends to extract four sets of features like Shannon entropy, Kapur entropy, Renyi's entropy, LBP and GLCM. The feature selection method, which chooses the distinctive characteristics with lower correlation, is carried out since it seems that the feature vector is lengthy. Then, using the FESO algorithm, the important features are chosen from the extracted features. As a result, the classifier PDDLSTM classifies the retinal fundus image using the selected features as input. The paper's major goal is to offer an automated DR detection method that is more accurate, uses less memory, and requires less computing time. By assessing measures like sensitivity, specificity, and accuracy, the performance of the proposed approach is verified using the openly available standard dataset DRIVE. The simulation results show that sensitivity, specificity, and accuracy of 0.95, 0.98, and 0.985 are achieved when comparing the performance of the proposed PDDLSTM algorithm with those of other optimisation techniques.

Keywords - Kirsch with Mask based Watershed Segmentation (KM-WS), Block-Matching and 3D (BM3D), Fisher Egret Swarm Optimization (FESO), Poisson Distributed Deep Long Short Memory (PDDLSTM) network, retinal fundus image and retinal disease classification.

1 INTRODUCTION

One of the most important instruments in the healthcare industry is medical imaging, which is used for various illnesses information extraction as well as record keeping and visual documentation [1][2]. Diabetes is a condition marked by elevated blood sugar levels. Different eye conditions, such as glaucoma, diabetic macular edoema, and diabetic retinopathy, which can cause total vision loss, are at risk for developing in victims. Retinal fundus imaging is the most often used method for diagnosing Diabetic Eye Disease (DED), which is the most frequent consequence of diabetes. Ophthalmologists often analyze the degree and intensity of DED associated with a patient's diabetes based on the lesion seen in retinal fundus images [3]. Because of this, accuracy in medical image analysis is crucial for applications based on healthcare [4], and targeted study is needed to create algorithms that are reliable. Retinal disorders have significantly increased public health concerns in recent years. They take time to grow and show no symptoms at first. Retinal illnesses affect millions of people worldwide each year, and they can manifest themselves in a number of different ways [5]. Retinal disease can affect any part of the retina, causing vision impairment and sometimes blindness. These include Diabetic Retinopathy (DR), macular spasms, glaucoma, Macular Hole (MH), Age-Related Macular Degeneration (AMD), drusen, Central Serous Retinopathy (CSR), macular edema, cataracts, and optic nerve abnormalities. Many diseases of the retina. These conditions include (i) loss of vision, (ii) floaters and cobwebs, (iii) flashing lights, (iv) objects appearing larger or smaller than they actually are, (v) decreased peripheral vision or appearance of shadows and (vi) rectilinear distortion [6].

The procedure for classifying diabetic retinopathy using retinal color fundus image often includes preprocessing, blood vessels, optic disc segmentation, feature extraction, and image classification [7, 8]. Noise, refraction, blurring, illumination variations and low contrast are the main factors affecting fundus images. Therefore, multiple learning steps are used before classification to improve contrast and image quality. Most DR screening techniques use the Contrast Limited Adaptive Histogram Equalization (CLAHE) method to improve the contrast of fundus images and filtering techniques to reduce image noise [9]. A variety of anatomical structures are clearly visible on the color fundus image, including blood vessels, papilla, fovea, macular region, and abnormalities called lesions. Because papillae and blood vessels are of similar intensity to dark red lesions, they must be isolated and removed to effectively detect lesions for DR severity classification. Morphological, threshold, edge, and cluster-based methods are often used for papilla localization and vessel segmentation [10]. Also, feature extraction based on statistics, texture, shapes, color, and intensity is used by the examiner to explain the positive edges of an image before classification [11].

Most modern image processing techniques use model-integrated Deep Neural Networks (DNN), Convolutional Neural Networks (CNN), and Support Vector Machines (SVMs) to process images. Of course, it is often impossible to edit or prepare appropriate teaching

materials, so the specific image signal information is often fuzzy, noisy or missing. For this reason, predictive statistical methods or different branches of deep neural networks are often preferred [12, 13]. Although deep networks can be further trained on an existing model, the general principle still depends on that model, which reinforces a decision rule. These factors limit the dynamics of a system's adaptability.The training process is complicated because to its non-linear structure and the choice of the appropriate values for regulating factors like weights and biases. The main drawbacks of conventional training methods are local optima stagnation and poor convergence [14]. Combining deep learning architectures with bio-inspired optimization techniques increases classification accuracy with a high convergence rate while lowering model computing cost. They assist in the best feature choice for classification in addition to hyperparameter modification [15]. In order to enhance the classification performance of the created model, a novel training technique based on swarm optimization and deep learning was designed.

Problem Definition

- It is especially difficult to identify and separate smaller vessels because of the significant amount of noise and low lighting present. These noises, which result from different operational restrictions of the fundus imaging systems, include (systematic) additive noise and multiplicative (speckle) noise.
- Considering all the features for disease detection may provide the incorrect outcome and inaccurate result.
- The occlusion of vessels in the retina provides the worst detection rate.

To mitigate those problems this research methodology proposed an advanced approach with considering most important metrics for the eye disease segmentation and classification process. The research objectives of the presented research are given as follows,

- To segment the vessels by applying filter with considering KM-WS approach.
- To reduce the error of the disease classification by feature selection approach.
- To accurately classifies the diseases by using PDDLSTM approach.

The structure of the proposed research methodology is organized as follows, in section 2, the existing research methodologies related with the detection of medical conditions for eye disease is explained, in section 3, the proposed methodology has been explained, in section 4, the experimental analysis of the proposed methodology is given and in section 5, the proposed research is concluded with the future enhancement.

2 RELATED WORK

Research in the area of imaging and different imaging techniques have become very important for medical treatment and the early identification of medicalconditions has been to a variety of sophisticated imaging methods and algorithms provided by researchers to increase accuracy and precision.

Butt *et al.,* [16] suggested a thorough image-based method for diagnosing glaucoma.Retinal fundus glaucoma is recognized by a number of characteristics. To analyse depth images, these characteristics are combined with the majority of the data that was obtained, including cup-to-disc ratio, inferior, superior, nasal, and temporal area. With the use of this suggested approach, the ophthalmologist may better assess numerous glaucoma indicators in retinal fundus images.

Gampala *et al.*, [17] have investigated an effective in detecting glaucoma using Deep Neuro Fuzzy Network (DNFN). The initial input for denoising preprocessing consists of retinal images. Then the Optic Disc (OD) was detected using the fuzzy black hole entropy clustering algorithm or the deep seal model. DNFN based OD and blood vessels are adjusted before training with the new Multiverse Rider Wave Optimization (MVRWO). Multiverse optimizer, driver optimization algorithms and water wave optimization are integrated in the new MVRWO.

Mutukannan *et al.*, [18] investigated the early detection of age-related eye problems using retinal fundus images from an online dataset preprocessed with maximum entropic transformation. The pre-processed images were loaded into a Convolutional Neural Network (CNN) augmented with a Flower Pollination Optimization (FPOA) algorithm for feature extraction. Hyperparameters were optimized using FPOA for CNN training. This increased the accuracy and efficiency of the network. From the CNN output, a Multiclass Support Vector Machine (MSVM) classifier was used to identify disease type.

Al-Gburi *et al.*, [19] presented three integrated methods based on the Golden Eagle algorithm, the backup vector machine, the geometrically active contour technique and image segmentation. To test these methods, the popular RIM-ONE Retina benchmark database was used. In this study, pre-processing based on geometrically active Shannon contours and post-processing based on regularly spaced cross-sectional segmentation controlled by the Golden-Eagle algorithm are used. The Golden Eagle methodology is superior to approaches such as the geometrically active contour and the SVM technique.

OCT images using CNN and the thin mold method based detection of retinal diseases were developed by Togakar *et al.,* [20]. For each model in the recommendation strategy, class-based activations were extracted using the data set and nine transfer learning models. SMA was used to select the dominant activations among the model-based activations of each class, and then the selected activations were ranked using the Softmax method.

3 RESEARCH METHODOLOGY

A novel technique has evolved for the identification of retinal diseases utilizing computer-aided diagnostics using fundus images. However, there are still issues with getting an accurate disease detection process. Therefore, this research methodology suggested a PDDLSTM-based method for detecting retinal diseases. The input image is first processed to obtain the green fundus channel. The green channel has been removed as it provides more information about the retinal background image.From the extracted green channel, the filter is

removed using BM3D approach. Then, the vessel and other parts of the retinal image are extracted by using the KM-WS approach. Then, features are extracted from the extracted features the important features are selected using FESO algorithm. Thus, the selected features are given as input to the classifier PDDLSTM it classifies the retinal fundus image as, normal, Background Diabetic Retinopathy (BDR), Proliferative Diabetic Retinopathy (PDR), Hypertensive Retinopathy (HR), Coat's Disease (CD), and Retinitis. In figure 1 shows that the proposed block diagram has been illustrated.

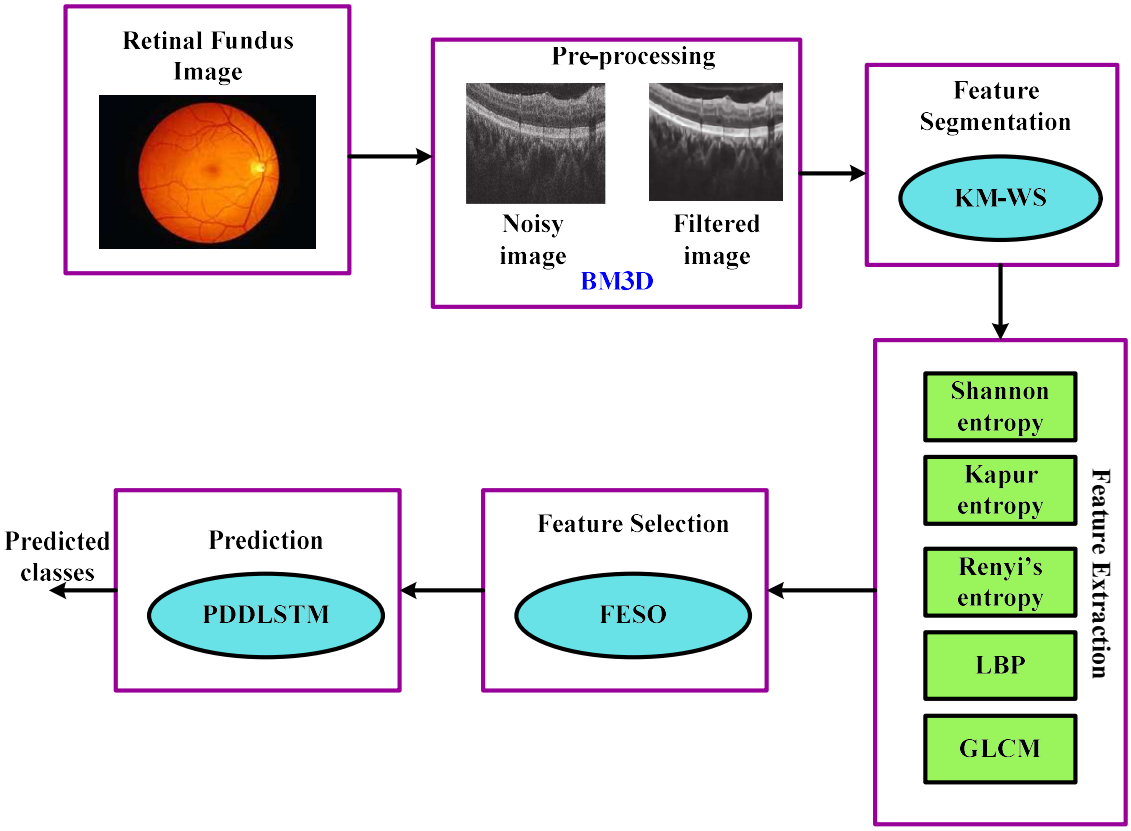

Figure 1 Block diagram for the proposed research methodology

3.1 Filtering Method

In the first step, the Block-Matching and 3D (BM3D) algorithm was applied to the OCT images to reduce noise. The BM3D algorithm has higher superiority and effectiveness than conventional filtering methods on OCT images. It entails identifying a collection of related patches in non-local OCT image areas and obtaining a 3-D wavelet representation of the patch group, respectively [21]. The BM3D algorithm's primary structure could be broken down into two distinct parts. The first stage, which has three sub-steps, uses hard thresholding during collaborative filtering to estimate the de-noised image.

$$\Re(\Re)_{Hard} = \alpha^{3D}_{Hard-1} * \left(\omega\left(\alpha^{3D}_{Hard-1}(\Re(\Re))\right)\right) \quad (1)$$

When β a hard thresholding operator with threshold is ω used, the designation of zero signifies that Gaussian noise variance.

$$\omega(i)=\begin{cases}0 & if\ |i|\le \alpha_{Hard}^{3D}\beta \\ i & otherwiase\end{cases}$$

(2)

The patches of the concurrently filtered 2D images look the final 3D block. The aggregate procedure, which comes last, provides an estimate for each patch that has been utilized. These projections are kept in a buffer.

$$\forall \aleph \in \Re(\Re), \forall i \in \aleph, \begin{cases}\tau(i)=\tau(i)+k_{Hard}^{\Re} j_{Hard}^{\aleph,\Re}(i) \\ \eta(i)=\eta(i)+k_{Hard}^{\Re}\end{cases}$$

(3)

Where, the numerator and denominator parts of the basic estimate of the image obtained at the end of the grouping step are denoted as τ and η respectively. $j_{Hard}^{\aleph,\Re}$ specify the estimated pixel value i that was obtained through collaborative filtering.

$$k_{Hard}^{\Re}=\begin{cases}\left(\mathrm{P}_{Hard}^{\Re}\right)^{-1} & if \mathrm{P}_{Hard}^{\Re}\ge 1 \\ 1 & otherwise\end{cases}$$

(4)

Like the $\mathrm{P}_{Hard}^{\Re}$ non-zero coefficients that was attained following rigorous thresholding in the aforementioned 3D block. The basic estimate that was generated after this first phase is given by equation (5) below.

$$j_{basic}(i)=\frac{\sum_{\Re} k_{Hard}^{\Re} * \sum_{\aleph\in\Re(\Re)} I\aleph(i) j_{Hard}^{\aleph,\Re}(i)}{\sum_{\Re} k_{Hard}^{\Re} * \sum_{\aleph\in\Re(\Re)} I\aleph(i)}$$

(5)

To get this estimate, the numerator and denominator of the two buffers are simply divided element by element according to the next condition.

$$I\aleph(i)=\begin{cases}1\ if\ and\ only\ if\ i\in\aleph \\ 0 \quad otherwise\end{cases}$$

(6)

Wiener filtering is used in the second major phase. With two variations taken into consideration, this second phase mimics the first one. The filtered patches are compared, not the original patches. The new 3D group is analyzed using Wiener filtering instead of simple thresholding. This step executes the sub-actions defined by Grouping, Collaborative Filtering,

and Aggregation.The patch-matching is handled on the basis of the fundamental estimate j_{basic} during the grouping procedure. In actuality, a collection of related patches is gathered to create 3D groups.

$$\Re_{Basic}(\Re) = \{\aleph : d(\Re,\aleph) \le \gamma_{wiener}\} \tag{7}$$

The base score and the original noise image $\Re_{Basic}(\Re)$ and $\Re(\Re)$are used to create similar patches after overlay. γ_{wiener} is the distance at which two patches are deemed to be identical for d. Once the 3D blocks have been located and grouped, the collaborative filtering process can begin. Wiener filtering is used to carry out the filtering process $\Re(\Re)$ known as Wiener collaborative filtering. The 3D transformations of the noisy image are actually multiplied by the Wiener coefficients, which are specified as follows, to create the final image.

$$k_{\Re}(\varepsilon) = \frac{\left|\gamma_{wiener}\left(\Re_{Basic}(\Re)\right)(\varepsilon)\right|^2}{\left|\gamma^{3D}_{wiener^{-1}}\left(\Re_{Basic}(\Re)\right)(\varepsilon)\right|^2 + \beta^2} \tag{8}$$

Equation (9) provides the 3D group's estimate.

$$\Re_{wiener}(\Re) = \gamma^{3D}_{wiener^{-1}}\left(k_{\Re}.\gamma^{3D}_{wiener^{-1}}\left(\Re(\Re)\right)\right) \tag{9}$$

Aggregation, which occurs when collaborative filtering is successful, is the final quick stage. The estimate for each pixel is the value that this step requires to save in a buffer.

$$\forall \aleph \in \Re(\Re), \forall i \in \aleph, \begin{cases} \tau(i) = \tau(i) + k^{\Re}_{wiener} j^{\aleph,\Re}_{wiener}(i) \\ \eta(i) = \eta(i) + k^{\Re}_{wiener} \end{cases} \tag{10}$$

Where, the components of the final assessment image that was obtained at the conclusion of the numerator and denominator is denoted by γ and η. $j^{\aleph,\Re}_{wiener}(i)$ is the pixel i value from the patch $\aleph$ that was created by filtering the reference patch.

$$k^{\Re}_{wiener} = \left\|k_{\Re}\right\|_2^{-2} \tag{11}$$

The following equation results in the final estimate image:

$$j_{Final}(i) = \frac{\sum_{\Re} k^{\Re}_{wiener} \sum_{\aleph \in \Re(\Re)} I\aleph j^{\aleph,\Re}_{wiener}(i)}{\sum_{\Re} k^{\Re}_{wiener} \sum_{\aleph \in \Re(\Re)} I\aleph(i)} \tag{12}$$

Following the first step, the final estimate is determined by dividing the numerator and denominator of the elements of the two buffers by the elements that relate to the circumstances stated in equation (12). The size of the BM3D denoises is determined by the threshold coefficients used. The property that is chosen has an impact on how much information is available. Despite the fact that there are several search design strategies accessible, only three viable ones will be taken into account in this study to determine which is best for each kind of quality. The BM3D is summarized in Figure 2.

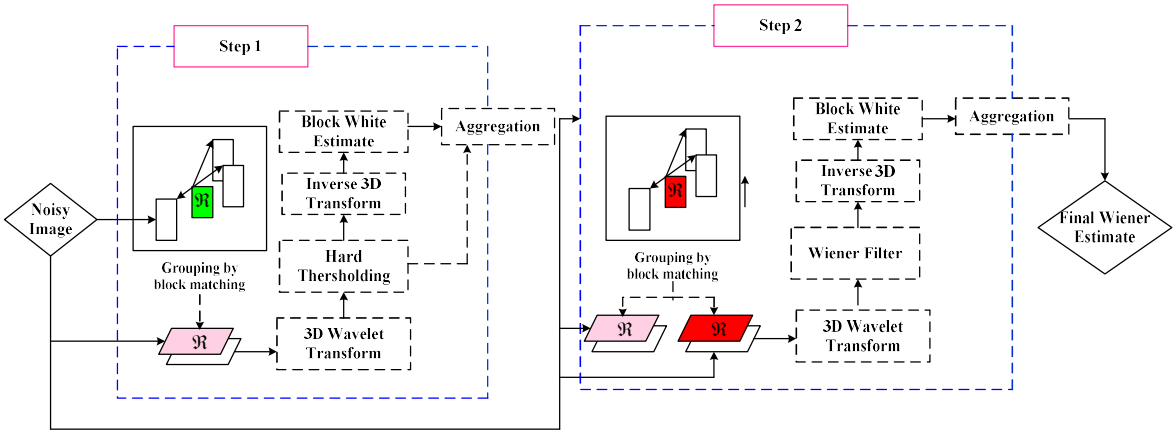

Figure 2 Structure of Block-Matching and 3D approach

3.2 Segmentation

For the segmentation process this research methodology uses the Kirsch with Mask based Watershed Segmentation (KM-WS) approach. If the vessel has an occlusion, then effectively the vessels are segmented by using the Kirsch approach. First, the Kirsch template-based edge detection; false edge removal, vessel junction restoration, and vessel labelling process are carried out.

Kirsch with Mask algorithm

For edge detection, the Kirsch approach is used on preprocessed images which are yield the greatest value when taken into account as the structuring component for edge detection. The Kirsch edge detection method recognizes the existence of an edge as well as its direction [22]. North, northeast, east, southeast, south, southwest, west, and northwest are the eight directions that can be taken.

- Rotate a single mask in the directions of the north, northeast, east, southeast, south, southwest, west, and northwest compass needles.
- An edge's magnitude determined by convolutioning each mask's highest value with the image.
- The mask that yields the largest magnitude determines the direction of the edge.

The following is an explanation of Kirsch masks:

$$East=\begin{pmatrix}-3 & -3 & -3\\ -3 & 0 & -3\\ 5 & 5 & 5\end{pmatrix} \quad Southeast=\begin{pmatrix}-3 & -3 & -3\\ 5 & 0 & -3\\ 5 & 5 & -3\end{pmatrix} \quad Northwest=\begin{pmatrix}-3 & 5 & 5\\ -3 & 0 & 5\\ -3 & -3 & -3\end{pmatrix}$$

$$West=\begin{pmatrix}5 & 5 & 5\\ -3 & 0 & -3\\ -3 & -3 & -3\end{pmatrix} \quad North=\begin{pmatrix}-3 & -3 & 5\\ -3 & 0 & 5\\ -3 & -3 & 5\end{pmatrix} \quad Southwest=\begin{pmatrix}5 & 5 & -3\\ 5 & 0 & -3\\ -3 & -3 & -3\end{pmatrix}$$

$$Northeast=\begin{pmatrix}-3 & -3 & -3\\ -3 & 0 & 5\\ -3 & 5 & 5\end{pmatrix} \quad South=\begin{pmatrix}5 & -3 & -3\\ 5 & 0 & -3\\ 5 & -3 & -3\end{pmatrix}$$

(13)

For images with more contrast between the pixels in the foreground and background, the Kirsch method performs well. Twenty fundus images from each database were used to test the established threshold, and in each instance, we found it to be appropriate. In order to reduce the noise around the retrieved exudates, the obtained image is subjected to a morphological opening procedure, as indicated in equation (14).

$$V_Q=(V\ \theta\ Q)+Q$$

(14)

Consider that the structural element Q and V the object V are first corroded and then enlarged Q. The acquired resulting image is used to extract the final exudates. When erosion is followed by dilation in animage, the noise outside of the object is removed using the morphological opening operation, which has been assessed by equation (13), utilizing a comparable structural element for both procedures. The watershed technique is then used to remove vessels from the image of the retinal fundus.

Watershed Segmentation

The watershed segmentation technique is used to create spots in an image by adjusting the size of the gradient. If the minimum and maximum of the image feature of interest are feature boundaries, this method provides a powerful segmentation tool. The input image for this step is usually agradient image. Thus, the space between the watershed is marked by lines that form edges and basins. Depending on the pixel level, the image is divided into areas by merging white pixels. When a gradient image is used as an input image, the segmentation generates a water transition that can be visualized as a closed circle in the segmented area [23]. One of the main options for using the water separation method is medical image processing. For example, the ability to distinguish between light and dark areas on MRIs can aid in diagnosis. This can be achieved by re-segmenting the image using watershed segmentation.

3.3 Feature Extraction

After segmentation comes a feature extraction process, which is one of the most important image processing techniques to redefine large redundant data into small features. From the segmented image, the amount of exudate, separation between two blood vessels, Shannon's entropy, Kapoor's entropy, René's entropy, LBP, and grayscale compatibility matrix (GLCM) properties are extracted. Sorting capabilities are tested through extensive computer simulations to find the most unique identifiers that complement the best recognition performance.

GLSM

Here, we extract two blood vessel characteristics, color, GLCM, and form. The most important aspect that has been shown to be an ideal quantity for improved fundus image categorization with its form is compression is the shape of two blood vessels. According to ophthalmologists, the fundus image's form properties are a more crucial characteristic for discriminating [24]. The fundus image shape analysis method extracts the boundary and region-based characteristics. A probability distribution is described by a second-order statistic involving the probability that two pixels with a given gray level appear in some spatial relationship. These data, calculated using various orientations and separations, are displayed in two-dimensional gray-level display matrices.

In addition to the above-described elements, we have also employed the following two blood vessel-based features. The energy of the cells, called the volume unit, is an important factor in laboratory imaging.Where the word "feature" λ is defined.

$$\lambda = \sum_{j}\sum_{k}\alpha^{2}(j,k)+\left(\sqrt{-1}\right)*\left(\frac{\sqrt{\sum_{j=1}^{l}\left(c_{j}-c'\right)^{2}}}{l-1}\right) \tag{15}$$

Thus, the normalized GLCM element for the jth row and kth column is represented as $c' = \sum_{j=1}^{k}\frac{c_{j}}{l}, \alpha(j,k)$.

LBP

It is advised as a reliable and effective texture descriptor that might be used in a variety of applications, from face recognition to texture segmentation. The LBP operator categorizes the image pixels by thresholding the area around each pixel with the centre value, and this thresholding output is taken as the binary value [25]. After each pixel is classified according to the LBP codes, a label histogram $LI_{ABN}(i,j)$is calculated and used as a description of the texture. If Q is true $L(Q)=1$and Q is false $L(Q)=0$, and $L(Q)=1$is the number of unique

labels returned by the LBP operator, the histogram of the labeled image is used as description and comparison using equation (16)

$$\Delta_{HS}(Pic)=\sum_{i,j} L(LI_{ABN}(i,j)=pic), pic=0,.....,k-1 \quad (16)$$

Additionally, a pixel's neighborhood is captured in a circle. α Points with radius γ are chosen throughout the circle's perimeter. Utilizing Eq. (17), the uniformity metric $(\Delta_{UM})$is calculated by utilizing $\Delta_{LBP}(\alpha,\gamma)$a α -bit binary value $(b_{\alpha-1},b_{\alpha-2},....,b_1,b_0)$ to provide a uniform pattern that is rotation-invariant with finer angular quantization.

$$\Delta_{UM}(\Delta_{LBP}(\alpha,\gamma))=|b_{\alpha-1}-b_0|+\sum_{\alpha=1}^{\alpha-1}|b_\alpha-b_{\alpha-1}| \quad (17)$$

Where, $\Delta_{gv}(cp)$ denotes the gray value of the center pixel, α denotes the gray values of the points, and $\Delta_{gv}(cp), \alpha=0,.....,\alpha-1$. In equation (17), a value less than or equal to 2 gives a homogeneous pattern Δ_{UM} rotation model. A multi-scale assessment is carried out using LBP by choosing circles of different radii around the centre pixels and producing a different LBP image for each size. Additionally, the LBP image's energy and entropy, $S=1,2,$ *and* 3 which are constructed from a number of different pixel counts $\alpha=8,16,$ *and* 24 are used as feature descriptors.

$$\Delta_{LBP}(\alpha,S)=\begin{cases}\sum_{\alpha=0}^{\alpha-1} S(\Delta_{gv}(\alpha)-\Delta_{gv}(cp)) & if\ \Delta_{UM}(\Delta_{LBP}(\alpha,S))\le 2\\ \alpha+1 & otherwise\end{cases} \quad (18)$$

Entropy

A non-stationary signal decomposition method called Two-Dimensional Variational Mode Decomposition (2DVMD) is used to recover entropies [26]. To best pixel changes, the 2D-VMD repeatedly divides animage into a number of sub bands. To measure the regularity of pixels, intricate patterns, and finer features in the fundus images, three separate entropies of the normalized intensity histogram—Shannon entropy (Ψ_1), Renyi entropy (Ψ_2), and Kapur entropy (Ψ_3)—are recovered from the 2D-VMD modes. Using Eq. (19), the normalized intensity histogram IH_x^N is computed.

$$IH_x^N=\frac{\omega_x}{G\times H} \quad (19)$$

Where, ω_x represents the intensity values $x = 0,1,2,.....,\beta-1$, IH_x^N is the normalized intensity histogram's probability distribution, and $G \times H$ is the image's size.

Ψ_1 with the aid of equation (20),

$$\Psi_1 = -\sum_{x=0}^{\beta-1} IH_x^N \log 2\left(IH_x^N\right) \tag{20}$$

Utilizing Equation (21), Ψ_2 is calculated.

$$\Psi_2 = \frac{1}{1-k} \log \sum_{x=0}^{\beta-1} \left(IH_x^N\right) \tag{21}$$

where $k > 0 \Psi_3$ is determined by using Eq. (22)

$$\Psi_3 = \frac{1}{j-k} \log \frac{\sum_{x=0}^{\beta-1} \left(IH_x^N\right)^k}{\sum_{x=0}^{\beta-1} \left(IH_x^N\right)^j} \tag{22}$$

Where the number of grey levels is β.

3.4 Feature Selection

In order to extract meaningful independent information for a particular issue, feature selection decreases the quantity of linearly dependent characteristics. The three channels—red (R), green (G), and blue (B)—are employed to capture all of the information contained in the image, as opposed to earlier work on illness diagnosis using retinal fundus imaging, which often utilized the green channel of the RGB image. Additionally, since the textural features of the image are primarily based on the spatial repetition of any two adjacent pixels in the gray-level version of the image, we use that one as well. Utilizing the Fisher Egret Swarm Optimization (FESO) algorithm, the import features are chosen. Instead of employing random point generation, this study approach estimates the fisher score for the initialized population and uses that value. The typical egret swarm procedure has local optimum and convergence problems that need to be solved [27]. There are certain iterated processes in the proposed FESO-based feature selection and parameter optimization systems. The whole explanation is provided below.

Step 1: Preying behavior

Fish that are preying swim towards the direction of an area with plenty of food. Let ρ_k the artificial fish's current location be k^{th}, then use equation (23), which determines a random place ρ_l inside the fish's l^{th} visual range.

$$\rho_l = \rho_k + ran(\ ) * Visual \tag{23}$$

Step 2: Fitness calculation

Each solution's fitness is calculated after solution initialization. The goal of fitness is to reduce the connection between the characteristics. In the beginning, the features must be chosen so that there is the least possible correlation between them. A higher degree of accuracy may be determined if there is little to no association between the characteristics. Where, NP is the number of pairs of features, defines the relationship between two features γ and δ has been determined by equation (24). The minimization function is regarded as the best fitness in this study. Equation (24) contains the fitness function.

$$FF = Min(C) \tag{24}$$

Where,

$$C = \frac{NP\sum\gamma\delta - \sum\gamma\sum\delta}{\left(\sqrt{NP\sum\gamma^2 - \left(\sum\gamma\right)^2}\right) - \left(\sqrt{NP\sum\delta^2 - \left(\sum\delta\right)^2}\right)} \tag{25}$$

FF is the fitness function, and C are the correlation.

Step 3: Updating function using Egret Swarm Optimization

When the hybrid FESO algorithm is operating, each feature subset, the FSO local-decision range, and its update rule will be converted from an ESO-update phase that is into a movement-phase, aiding in the feature subset determination. After an FSO procedure and its conversion of the great and snowy egrets into feature subset egrets, the feature subset is established. The results demonstrate that FESO feature selection combined with parameter optimization has increased performance. According to equation (26), fish moves one step in the direction of the in the greatest problem if $FF_k < FF_l$.

$$\left[\rho_k^{rand}\right]^{ESO(\alpha,\beta,\gamma)} = \left[\rho_k\right]^{ESO(\alpha,\beta,\gamma)} + \left[rand(\ ) * visual\right]^{ESO(\alpha,\beta,\gamma)} \tag{26}$$

General working of ESO

Three main components of the predatory behavior of snow-white and great egrets, the "sit and wait" strategy, the aggressive strategy, and the discriminatory state, are the motivation for ESO [28]. Each n group of teams of egrets in the egret population consists of three egrets. Egrets α use a "sit and wait" approach, while aggressive egrets β use erratic walking and circling is γ.

The function E describes the Egret's α technique of evaluating potential targets at its current location, and a_m is the group m's position, $\mathrm{Y}_m = E(a_m)$ in the observation equation for the mth Egret α. Determine the error Er_m, parameterize the evaluation process, and iteratively determine the current estimate value of the prey Y_m.

$$\mathrm{Y}_m = wt_m * a_m \tag{27}$$

$$Er_m = \frac{\left\| \mathrm{Y}_m - \overline{\mathrm{Y}}_m \right\|^2}{2} \tag{28}$$

wt_m is the weighting used in the assessment process. $*$ signifies multiplication, the next sentence is same.

Egret's α most updated location is shown as follows:

$$a_{\alpha,m} = a_m + \exp\left(\frac{-i}{0.1 * i_{\max}} \right) * 0.1 * hop * wt_g \tag{29}$$

Where, i represents the current number of iterations, $i_{\max}$ represents the maximum number of iterations, wt_g weight is the gradient and the hop is the D-value of the position edge, so the hop value is equal to the edge of the lower solution from the edge of the upper solution.

The equation to update the position of the Egret is β:

$$a_{\beta,m} = a_m + \tan\left(R_{\beta,m}\right) * hop / (1 + i) \tag{30}$$

$\left(-\pi/2, \pi/2,\right)$ in which a random number is $R_{\beta,m}$. The egret γ uses the encirclement tactic. When it locates its prey, it pursues it until it is captured.

$$a_{\gamma,m} = (1 - R_m - R_n) * a_m + V_f + R_n * V_g \tag{31}$$

Where, V_f is the difference matrix between the current location of the egret swarm and the optimal location, and V_g is the matrix between the current location and the ideal location of the egret population. R_m and R_n are random number between [0,0,5].

Step 4: Swarming behavior

The spontaneous grouping of fish to escape danger is referred to as swarming behavior. If $D_{kl} < Visual$, locate other artificial fish inside the artificial fish's field of view k^{th}, determine their centre location ρ_{Cent}, and count their number. Equation (32) states that the k^{th} fish advance one step if $O_{Con}/e_{Fish} > \sigma O_k$, which denotes a high food concentration and the absence of crowding in the field close to the neighborhood centre ρ_{Cent}.

$$\rho_k^{rand} = \rho_k + rand(\ ) * step * \frac{\rho_{cent} - \rho_k}{\left\| \rho_{cent} - \rho_k \right\|} \quad (32)$$

If not, the aggressive behavior is used.

Step 5: Following behavior

The artificial fish will behave as follows while swimming in the direction of the greatest concentration of food. If $D_{kl} < Visual$, locate more artificial fish in the k^{th} artificial fish's range of view, count the number there are ρ_k, and locate the artificial fish ρ_l with the highest value of the target function.

If $O_{Con}/e_{Fish} > \sigma O_k$, which indicates that there is a lot of food nearby and that the fish are not crowded in an area close to the location ρ_l, then, ρ_l in accordance with equation (33), j^{th} the fish moves one step forward.

$$\rho_k^{rand} = \rho_k + rand(\ ) * step * \frac{\rho_l - \rho_k}{\left\| \rho_l - \rho_k \right\|} \quad (33)$$

If not, the predatory behavior is used.

Step 5: Bulletin board

The ideal location of the artificial fish is noted on the bulletin board. The position of the artificial fish should be compared to the position recoded in the bulletin board after each evolution; if the position is better than the one in the bulletin board, the artificial fish will

replace the artificial fish in the bulletin board. Otherwise, nothing will change on the noticeboard. The best artificial fish is the one on the bulletin board, to sum up.

Input: Obtained features vector
Output: Selected features $\left[\rho_k^{rand}\right]=[0,1]$

Begin

Initialize population, fitness, iteration $i_{\min}$ and maximum iteration $i_{\max}$
Compute fitness
Set iteration $i=1$
While $\left(i \le i_{\max}\right)$ **do**
Preying behavior $\rho_l = \rho_k + ran(\ ) * Visual$,
Update the new position
If $\left[\rho_k^{rand}\right] \le a_m$ **{**
$a_m = a_{\alpha,m}$
} else {
$\alpha_m = a_{\beta m}$
} else {
$\alpha_m = a_{\gamma m}$
} end if
Obtain the Swarming behavior using $\rho_k^{rand} = \rho_k + rand(\ ) * step * \frac{\rho_{cent} - \rho_k}{\left\|\rho_{cent} - \rho_k\right\|}$,
Obtain the Following behavior using $\rho_k^{rand} = \rho_k + rand(\ ) * step * \frac{\rho_l - \rho_k}{\left\|\rho_l - \rho_k\right\|}$,
Calculate fitness
Set $i = i + 1$
End while
Return Cluster head
End

3.5 Classification

After the feature extraction and selection phase, the most important step is to classify the selected features.For disease classification this research methodology uses the Poisson Distributed Deep Long Short Memory (PDDLSTM) network. The conventional neural network has the time-consuming problem for the reason of storing all parameters. In order to solve that problem this research methodology the unwanted parameters are removed by the calculation of Poisson distribution function.

Sequence convolution layer convolution methods are applied to images of a given length after converting the sequence image into an image set. The sequence implementation layer converts the output of the convolution layer into sequence data for use in the LSTM network after convolution is triggered [29]. The main purpose of the convolution layer is indicated by the symbol $*$ (convolution operation). The convolution procedure uses input data and a programmable filter. The user can use an optional fill procedure on the convolution layer to modify the convolution region. The training filter can also have different dimensions 3×3 and 5×5. The primary purpose of rollup functions is to assign the function to the matching matrix and generate features that represent comparable geographic samples in the dataset. The discrete-time convolution function for 2D data is described as:

$$(I*F)(x,y)=\sum_{p}\sum_{q}F(p,q)S(x-p,y-q) \tag{34}$$

Here, I and F represent the inputs and the trainable filters, respectively. Deep learning models employ the Batch Normalization (BN) layer to speed up network setup and cut down on training time. The vanishing gradient issue is further lessened by using operations on the BN layer. By adding the variance of the input data is $VarMin_B$ and the mean of the mini-batch is Min_B, the BN layer output can be O_x calculated:

$$I'_x=\frac{i_x-Min_B}{\sqrt{VarMin_B^2+\Delta}} \tag{35}$$

$$O'_x=\mu alI'_x+\lambda \tag{36}$$

This I'_x is the normalized activation, and if the $VarMin_B$ result is extremely little, Constant Δ is used to balance the numbers. During optimization, μ the learnable parameters scale variable and balance variable λ are changed for optimal O'_x performance. A sigmoid and tangent function can result in gradient cancellation and explosion issues in big networks, such as deep learning models. An activation function that is frequently used is a corrected linear unit layer (ReLU). The ReLU level is determined as follows:

$$F(x)=Max(0,x) \tag{37}$$

Equation (37), states that if the input data is negative, it equals zero; else, it equalizes to the output. An LSTM with units that have a regulated structure made up of three gates (input, output, and forget) is an example of a recurrent neural network (RNN) model. These gates regulate the data flow in the units, and they retain data decided in a previous period in the deep

LSTM unit shown in Figure 3. Additionally, the gradient vanishing and explosion issues are greatly diminished by the DLSTM layer.

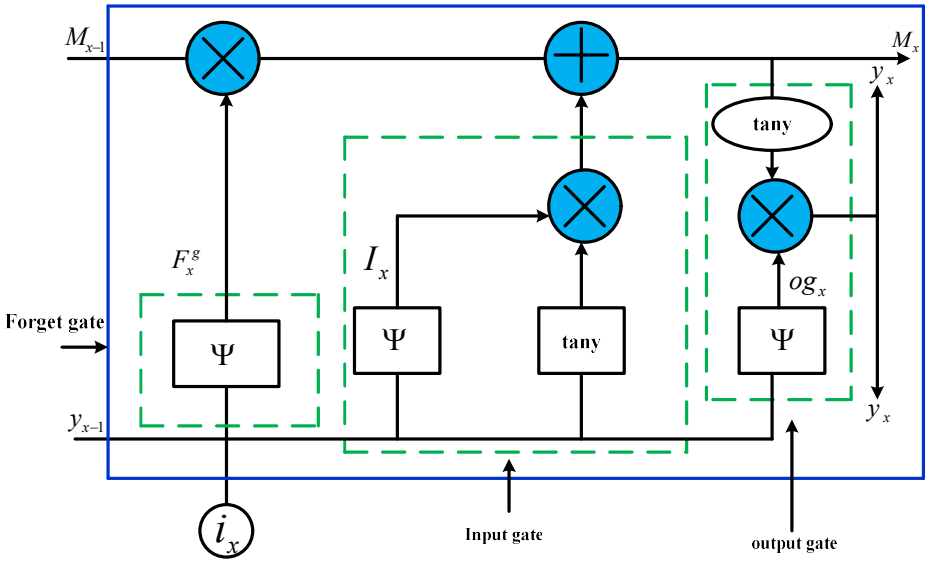

Figure 3 Procedure of the DLSTM Network

The forget gate structure and the Poisson Distributed Deep Long Short Memory (PDDLSTM) network are comparable. According to Equation (38), the forget gate opens if the output is equal to 1.

$$F_x^g = \Psi\left(Wt\left[i_x, y_{x-1}, M_{x-1}\right] + B_F\right) \tag{38}$$

Where, B_F represents the biased values, Ψ represents the sigmoid activation function, Wt represents the weighted vector, i_x and y_{x-1} are stand for the input and output vector of an earlier LSTM unit, and M_{x-1} stand for the earlier LSTM unit's memory.

The input gate is made out of a structure where the previous recollection unit data and a PDDLSTM are combined. Equations (39) and (40) express these calculations.

$$I_x = \Psi\left(Wt\left[i_x, y_{x-1}, M_{x-1}\right] + B_F\right) \tag{39}$$

$$M_x = F_x^g * M_{x-1} + I_x \cdot \tan y\left(\left[i_x, y_{x-1}, M_{x-1}\right]\right) + B_m \tag{40}$$

The connected LSTM device transmits data and information to the output gate. The computations carried out in the output gate are provided by equations (41) and (42).

$$\Psi_x = \Psi\left(Wi\left[i_x, y_{x-1}, M_{x-1}\right] + B_{og}\right)$$
(41)

$$y_x = og_x . \tan y\left(M_x\right)$$
(42)

The final estimated two-dimensional Poisson noise is created by combining the sounds from all layers of the deep convolution network with the noises produced by multi-directional LSTM networks, as shown in equation (43). An MLP (multilayer perceptron) is similar in structure to the FC layer [30]. The neurons in the FC layer provide suggestions as to how well a value fits any class. The dropout layer randomly changes input units to 0 at a frequency of rate at each step during training in order to avoid overfitting. The softmax layer uses class possibility values to classify data from the final FC layer. The softmax function is used in the CNN classification stage. The softmax function is written as follows:

$$SM_n = \frac{\Omega^{i_n}}{\sum_{n=1}^{k} \Omega^{i_n^k}}$$
(43)

For each input value (Ω^{i_n}), the output vector SM_n is computed, and the sum of all the output values equal to 1. The performance evaluation of the proposed method is explained in detail in the section below.

4 RESULTS AND DISCUSSION

The established DR detection method was implemented in MATLAB 2022a, and the suggested model's performance was assessed. This experiment used the DRIVE dataset, which contains 89 color fundus images. In this image, specialists detected areas containing microaneurysms, haemorrhages, hard exudates, and soft exudates [31]. To test the feature selection, the population size was set to 10, and the maximum number of iterations was determined as 100. Evaluation of "performance measures such as accuracy, sensitivity, specificity, precision, F1 score, and error rate" was done to compare the performance of the developed PDDLSTM to that of the traditional Learning Curved Layered Deep Learning Neural Network (LCL-DLNN), Deep Belief Networks (DBN), Convolutional Neural Network (CNN), and Recurrent Neural Network (RNN) techniques. Figure 4 illustrates the analysis performed on the input image, the filter image, and the segmented image.

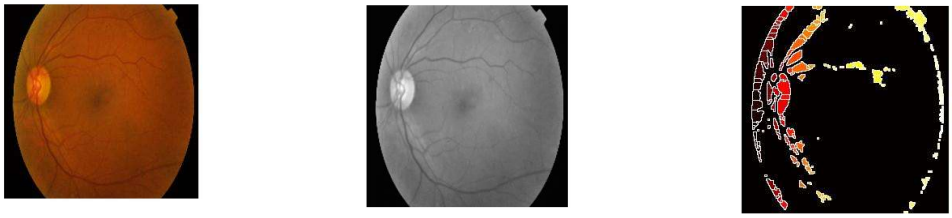

(a) (b) (c)

Figure 4 (a) Input image (b) Filter image and (c) Segmented image (DRIVE)

4.1 Performance analysis metrics

The blood vessel segmentation image is compared to the related ground truth image to determine the quantitative performance of the proposed work. The contrast between properly categorised background values (TN: True Negative) and foreground values (TP: True Positive) and incorrectly classified background values (FN: False Negative) and foreground values (FP: False Positive) determines how retinal images are categorised. Sensitivity (SEN), specificity (SPC), and accuracy (ACC) are used to evaluate the suggested approach.

Accuracy

One of the most often utilised measures to assess the efficacy of the segmented outcome is accuracy. It demonstrates how adept the system is at distinguishing between background pixels and the vessel. It is defined as the percentage of background and vessel pixels that were successfully recognised out of all the pixels in equation (44),

$$ACC = \frac{TP + TN}{FP + FN + TP + TN} \tag{44}$$

Sensitivity

It is the percentage of diabetic patients which have been categorised as true positives to all diabetic patients. It is often referred to as the genuine positive rate or recall. The evaluation is as follows:

$$SEN = \frac{TP}{TP + FN} \tag{45}$$

Specificity

The percentage of illnesses reported as being accurately ill is known as the specificity or TN rate. The evaluation is as follows:

$$SPC = \frac{TP}{TP + FN}$$

(46)

Precision

Precision (PR), as shown in equation (47) measures the level of categorization certainty.

$$PR = \frac{TP}{TP + FP}$$

(47)

F1-Score

Another method to evaluate the model's correctness is the F1-score, which is the harmonic mean of Sensitivity and Precision. The Dice Similarity Coefficient (DSC) is another name for it, and equation (48) may be used to compute it.

$$F1 - SCORE = \frac{TP}{TP + FP}$$

(48)

The performance comparisons between the proposed PDDLSTM and more established techniques, including LCL-DLNN, DBN, CNN, and RNN, are shown graphically in Figure 5. When compared to other conventional algorithms, the accuracy of the developed PDDLSTM is calculated effectively from Figure 5(a). The suggested PDDLSTM is 0.985, LCL-DLCNN is 0.98, DBN is 0.92, CNN is 0.65, and RNN is 0.69 with a learning rate of 65%. In a similar manner, Figure 5(b) shows the sensitivity. In addition, the specificity of the proposed PDDLSTM is shown in Figure 5(c). Therefore, the specificity of the proposed PDDLSTM is 0.002 higher than LCL-DLCNN, 0.05 higher than DBN, 0.21 higher than CNN, and 0.19 higher than RNN with 100% learning rate.

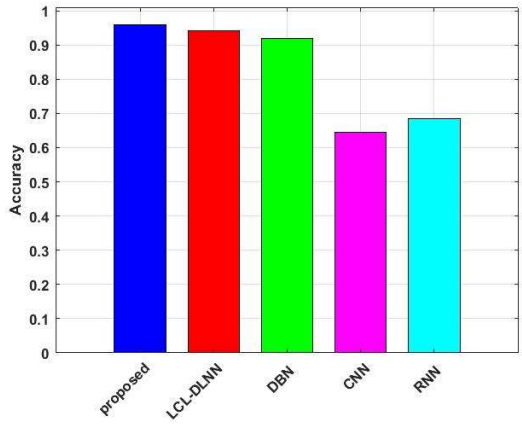

(a)

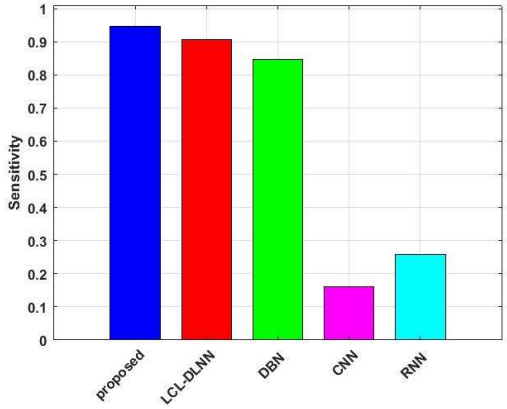

(b)

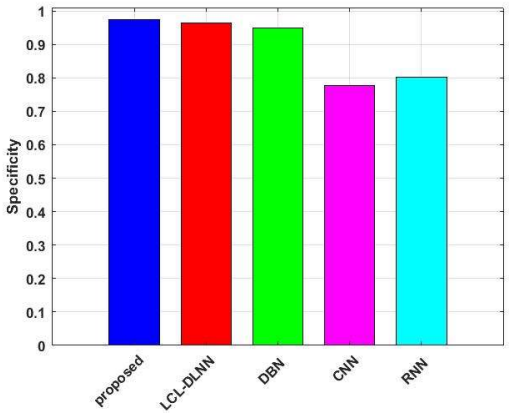

(c)

Figure 5 Graph representations of (a) Accuracy (b) Sensitivity and (c) Specificity

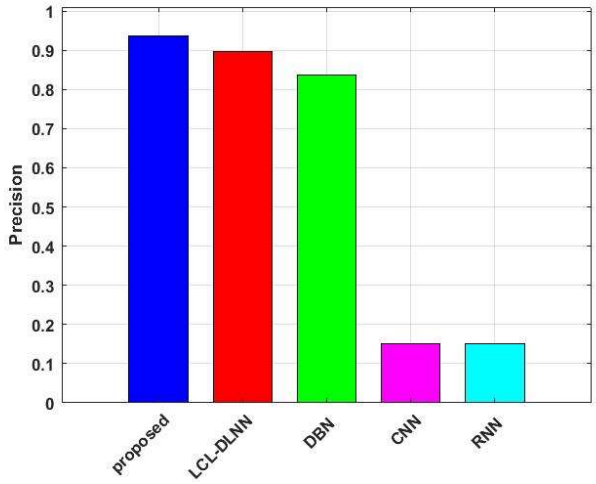

(a)

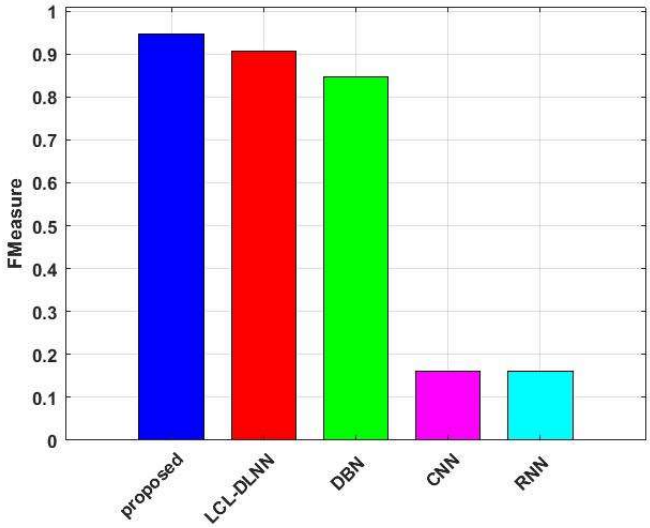

(b)

Figure 6 Graph representations of (a) Precision and (b) F1-Score

The accuracy and F-measure values of the suggested and current research approaches are shown in Figure 6. While recall gauges the quantity of performance, precision gauges the quality of performance. The F-Measure combines the sensitivity and accuracy metrics. In comparison to the current methodologies, the proposed method's precision is greater than 0.95 and its F-measure is 0.96. Here, based on the both metrics the proposed achieves better performance than the existing methodologies. Finally, the implemented PDDLSTM has been shown to outperform successful DR detection.

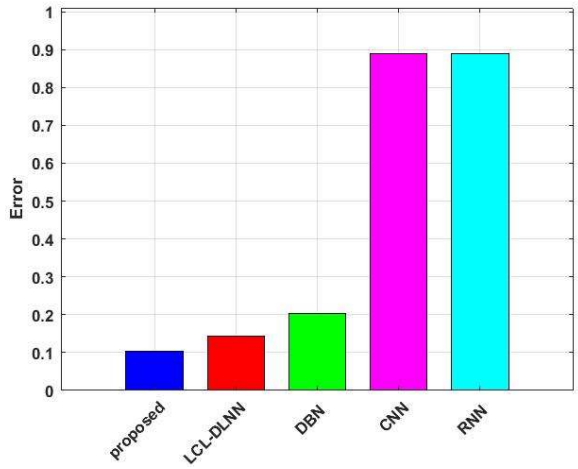

Figure 7 Output of Error value in proposed and existing methods

Table 1 Comparison analysis of previous work

Methods	Accuracy	Precision
LWDL [32]	0.96	-
HACO [33]	0.97	-
PSOLS [34]	0. 98	0.934
RNN	0.68	0.16
CNN	0.65	0.15
DBN	0.92	0.85
LCL-DLNN	0.98	0.9
Proposed PDDLSTM	0.985	0.95

Figure 7 depicts the comparative study of the suggested and current methodologies. In this case, the suggested technique performs better than current methods like LCL-DLNN, DBN, CNN, and RNN when the value is less than 0.1. Table 1 provides the past work

comparison based on categorization findings. Different performance metrics, like accuracy and precision, are used to assess the extent to which the suggested fundus image classification performs. We have used a variety of cutting-edge techniques in this experiment, including Light Weight Deep Learning (LWDL), Hybrid Ant Colony Optimisation (HACO), Particle Swarm Optimisation with Local Search (PSOLS), RNN, CNN, DBN, LCL-DLNN, and suggested optimum PDDLSTM. Finally, when compared to all other state-of-the-art methods, the proposed PDDLSTM based classification achieved higher performances.

5 CONCLUSION

The detection and classification of retinal disease using the KM-WS method and PDDLSTM is suggested in this research. The DR processing steps in this case were pre-processing, optic disc removal, blood vessel removal, abnormality segmentation, and classification. Based on the retinal fundus image and the chosen features, both the detection and classification assessment are taken into consideration in this case. It is a two-step processing in which the first stage uses FESO to size an ideal set of feature vectors, aiding in the quickest possible convergence and the removal of redundant data. Finally, a proposed approach is used to classify the retinal fundus image. Comparing the performance of the suggested methodology to other research methodologies such as LCL-DLNN, DBN, CNN, and RNN. The objective function evaluation was performed using accuracy, sensitivity, specificity, correctness, F1 value, and error value. The suggested achieves over 0.99 accuracy and performs better than the previous methods based on all measures. Future feature vector optimization will aim to achieve 100% segmentation accuracy. Advanced machine learning or deep learning algorithms with selective iterations of the algorithms, also referred to as the anti-crime organization for the purpose of detecting public disorder.

REFERENCES

[1] Alqudah, Ali Mohammad. "AOCT-NET: a convolutional network automated classification of multiclass retinal diseases using spectral-domain optical coherence tomography images." Medical & biological engineering & computing 58 (2020): 41-53.

[2] Sunija, A. P., et al. "Octnet: A lightweight CNN for retinal disease classification from optical coherence tomography images." Computer methods and programs in biomedicine 200 (2021): 105877.

[3] Bogunović, Hrvoje, et al. "RETOUCH: the retinal OCT fluid detection and segmentation benchmark and challenge." IEEE transactions on medical imaging 38.8 (2019): 1858-1874.

[4] Thangaraj, Sumathi, Vivekanandan Periyasamy, and Ravikanth Balaji. "Retinal vessel segmentation using neural network." IET Image Processing 12.5 (2018): 669-678.

[5] Ngo, Lua, Jaepyeong Cha, and Jae-Ho Han. "Deep neural network regression for automated retinal layer segmentation in optical coherence tomography images." IEEE transactions on image processing 29 (2019): 303-312.

[6] Rani, B. M. S., et al. "Disease prediction based retinal segmentation using bi-directional ConvLSTMU-Net." Journal of Ambient Intelligence and Humanized Computing (2021): 1-10.

[7] Jebaseeli, T. Jemima, C. Anand Deva Durai, and J. Dinesh Peter. "Segmentation of retinal blood vessels from ophthalmologic diabetic retinopathy images." Computers & Electrical Engineering 73 (2019): 245-258.

[8] Perdomo, Oscar, et al. "Classification of diabetes-related retinal diseases using a deep learning approach in optical coherence tomography." Computer methods and programs in biomedicine 178 (2019): 181-189.

[9] Noh, Kyoung Jin, Sang Jun Park, and Soochahn Lee. "Scale-space approximated convolutional neural networks for retinal vessel segmentation." Computer methods and programs in biomedicine 178 (2019): 237-246.

[10] Tayal, Akash, et al. "DL-CNN-based approach with image processing techniques for diagnosis of retinal diseases." Multimedia systems (2021): 1-22.

[11] Yoo, Tae Keun, Joon Yul Choi, and Hong Kyu Kim. "Feasibility study to improve deep learning in OCT diagnosis of rare retinal diseases with few-shot classification." Medical & Biological Engineering & Computing 59 (2021): 401-415.

[12] Li, Di, and Susanto Rahardja. "BSEResU-Net: An attention-based before-activation residual U-Net for retinal vessel segmentation." Computer Methods and Programs in Biomedicine 205 (2021): 106070.

[13] Balasubramanian, Kishore, and N. P. Ananthamoorthy. "Robust retinal blood vessel segmentation using convolutional neural network and support vector machine." Journal of Ambient Intelligence and Humanized Computing 12 (2021): 3559-3569.

[14] Sunija, A. P., et al. "Octnet: A lightweight cnn for retinal disease classification from optical coherence tomography images." Computer methods and programs in biomedicine 200 (2021): 105877.

[15] Uysal, Esin, and Gür Emre Güraksin. "Computer-aided retinal vessel segmentation in retinal images: convolutional neural networks." Multimedia Tools and Applications 80 (2021): 3505-3528.

[16] Butt, Muhammad Mohsin, et al. "Diabetic Retinopathy Detection from Fundus Images of the Eye Using Hybrid Deep Learning Features." Diagnostics 12.7 (2022): 1607.

[17] Gampala, Veerraju, et al. "Glaucoma detection using hybrid architecture based on optimal deep neuro fuzzy network." International Journal of Intelligent Systems 37.9 (2022): 6305-6330.

[18] Muthukannan, P. "Optimized convolution neural network based multiple eye disease detection." Computers in Biology and Medicine 146 (2022): 105648.

[19] Al-Gburi, Zahraa Dawood Salman, and Sefer Kurnaz. "Optical disk segmentation in human retina images with golden eagle optimizer." Optik 271 (2022): 170103.

[20] Toğaçar, Mesut, Burhan Ergen, and Vedat Tümen. "Use of dominant activations obtained by processing OCT images with the CNNs and slime mold method in retinal disease detection." Biocybernetics and Biomedical Engineering 42.2 (2022): 646-666.

[21] Mezni, Ilhem, et al. "Automated identification of SD-optical coherence tomography derived macular diseases by combining 3D-block-matching and deep learning techniques." Computer Methods in Biomechanics and Biomedical Engineering: Imaging & Visualization 9.6 (2021): 660-669.

[22] Orujov, Farid, et al. "Fuzzy based image edge detection algorithm for blood vessel detection in retinal images." Applied Soft Computing 94 (2020): 106452.

[23] Jadhav, Ambaji S., Pushpa B. Patil, and Sunil Biradar. "Optimal feature selection-based diabetic retinopathy detection using improved rider optimization algorithm enabled with deep learning." Evolutionary intelligence 14 (2021): 1431-1448.

[24] Vimal, S., et al. "RETRACTED ARTICLE: A method of progression detection for glaucoma using K-means and the GLCM algorithm toward smart medical prediction." The Journal of Supercomputing 77.10 (2021): 11894-11910.

[25] Patel, Rajneesh Kumar, and Manish Kashyap. "Automated screening of glaucoma stages from retinal fundus images using BPS and LBP based GLCM features." International Journal of Imaging Systems and Technology 33.1 (2023): 246-261.

[26] Jainish, G. R., G. Wiselin Jiji, and P. Alwin Infant. "A novel automatic retinal vessel extraction using maximum entropy based EM algorithm." Multimedia Tools and Applications 79 (2020): 22337-22353.

[27] Xian, Sidong, et al. "A novel fuzzy time series forecasting method based on the improved artificial fish swarm optimization algorithm." Soft Computing 22 (2018): 3907-3917.

[28] Chen, Zuyan, et al. "Egret Swarm Optimization Algorithm: An Evolutionary Computation Approach for Model Free Optimization." Biomimetics 7.4 (2022): 144.

[29] Das, Sraddha, et al. "Deep learning architecture based on segmented fundus image features for classification of diabetic retinopathy." Biomedical Signal Processing and Control 68 (2021): 102600.

[30] Liu, Genwang, et al. "A Bayesian deep learning method for freeway incident detection with uncertainty quantification." Accident Analysis & Prevention 176 (2022): 106796.

[31] Saranya, P., et al. "Blood vessel segmentation in retinal fundus images for proliferative diabetic retinopathy screening using deep learning." The Visual Computer (2022): 1-16.

[32] Aurangzeb, Khursheed, et al. "An Efficient and Light Weight Deep Learning Model for Accurate Retinal Vessels Segmentation." IEEE Access 11 (2022): 23107-23118.

[33] Devarajan, D., S. M. Ramesh, and B. Gomathy. "A metaheuristic segmentation framework for detection of retinal disorders from fundus images using a hybrid ant colony optimization." Soft Computing 24 (2020): 13347-13356.

[34] Ramya, J., M. P. Rajakumar, and B. Uma Maheswari. "HPWO-LS-based deep learning approach with S-ROA-optimized optic cup segmentation for fundus image classification." Neural Computing and Applications 33 (2021): 9677-9690.